Class A Penicillin-Binding Protein-mediated cell wall synthesis promotes structural integrity during peptidoglycan endopeptidase insufficiency

Shannon G. Murphy[1,2], Andrew N. Murtha[1,2], Ziyi Zhao[1*], Laura Alvarez[3], Peter Diebold[2], Jung-Ho Shin[1], Michael S. VanNieuwenhze[4], Felipe Cava[3] and Tobias Dörr[1,2,5#]

[1] Weill Institute for Cell and Molecular Biology, Cornell, University, Ithaca, NY 14853, USA.

[2] Department of Microbiology, Cornell University, Ithaca, NY 14853, USA.

[3]The Laboratory for Molecular Infection Medicine Sweden (MIMS), Department of Molecular Biology, Umeå University, SE-901 87 Umeå, Sweden.

[4]Department of Molecular and Cellular Biochemistry and Department of Biology, Indiana University, Bloomington, IN 47405, USA.

[5] Cornell Institute of Host-Microbe Interactions and Disease, Cornell University, Ithaca, NY 14853, USA.

*present address:

Department of Biochemistry and Biophysics, University of California, San Francisco, San Francisco, CA 94158, USA.

[#] address correspondence to tdoerr@cornell.edu , ORCID ID: 0000-0003-3283-9161

Running title: Endopeptidase depletion effects on cell wall synthesis

Keywords: Peptidoglycan, autolysin, endopeptidase, M23, LysM, Penicillin-binding Protein, mreB, cell wall, Vibrio cholerae

Abstract

The bacterial cell wall is composed primarily of peptidoglycan (PG), a poly-aminosugar that is essential to sustain cell shape, growth and structural integrity. PG is synthesized by two different types of synthase complexes (class A Penicillin-binding Proteins [PBP]s/Lpos and Shape, Elongation, Division, Sporulation [SEDS]/class B PBP pairs) and degraded by 'autolytic' enzymes to accommodate growth processes. It is thought that autolsyin activity (and particulary the activity of endopeptidases, EPs) is required for PG synthesis and incorporation by creating gaps that are patched and paved by PG synthases, but the exact relationship between autolysins and the separate synthesis machineries remains incompletely understood. Here, we have probed the consequences of EP depletion for PG synthesis in the diarrheal pathogen *Vibrio cholerae.* We found that EP depletion resulted in severe morphological defects, increased cell mass, a decline in viability, and continuing (yet aberrant) incorporation of cell wall material. Mass increase and cell wall incorporation proceeded in the presence of Rod system inhibitors, but was abolished upon inhibition of aPBPs. However, the Rod system remained functional (i.e., exhibited sustained directed motion) even after prolonged EP depletion, without effectively promoting cell elongation. Lastly, heterologous expression of an EP from *Neisseria gonorrhoeae* could fully complement growth and morphology of an EP-insufficient *V. cholerae.* Overall, our findings suggest that in *V. cholerae,* the Rod system requires endopeptidase activity (but not necessarily direct interaction with EPs) to promote cell expansion and substantial PG incorporation, whereas aPBPs are able to engage in sacculus construction even during severe EP insufficiency.

Importance

Synthesis and turnover of the bacterial cell wall must be tightly co-ordinated to avoid structural integrity failure and cell death. Details of this coordination are poorly understood, particularly if and how cell wall turnover enzymes are required for the activity of the different cell wall synthesis machines. Our results suggest that in *Vibrio cholerae*, one class of turnover enzymes, the endopeptidases, are required only for substantial PG incorporation mediated by the Rod system, while the aPBPs maintain structural integrity during endopeptidase insufficiency. Our results suggest that aPBPs are more versatile than the Rod system in their ability to recognize cell wall gaps formed by autolysins other than the major endopeptidases, adding to our understanding of the co-ordination between autolysins and cell wall synthases. A detailed understanding of autolysin biology may promote the development of antibiotics that target these essential turnover processes.

Introduction

Most bacteria elaborate a cell wall composed primarily of peptidoglycan (PG), which consists of polymerized N-acetyl glucosamine-N-acetyl muramic acid (poly-GlcNAc-MurNAc) dimers. These polymerized strands are covalently linked to each other via their oligopeptide side stems extending from the MurNAc residues; the degree of crosslinking varies with bacterial species and growth conditions (1-3). As such, PG encases the cell in a net-like structure that functions to maintain the high intracellular pressure accumulating in most bacteria and thus to prevent the cell from lysing. In

74 concert with maintenance of structural integrity, PG has to accommodate growth
75 processes (cell elongation and size expansion) and is therefore constantly degraded
76 and resynthesized (4-6).
77
78 In many rod-shaped Gram-negative bacteria, cell wall synthesis during cell elongation is
79 mediated by two separate types of cell wall synthase complexes: the Rod complex
80 (which includes the glycosyltransferase RodA in conjunction with a class B Penicillin-
81 Binding Protein [bPBP] and accessory proteins) and the class A PBPs in conjunction
82 with their lipoprotein activators (7-12). The differential physiological roles of these PG
83 synthases have only recently been begun to be dissected (13, 14), but remain
84 incompletely understood.
85
86 Cell wall degradation, on the other hand, is mediated by a plethora of so-called
87 “autolysins”, *i.e.*, enzymes with the capability to break bonds in the PG sacculus (15-
88 17). Members of one such group of autolysins, the endopeptidases (EPs), cleave the
89 oligopeptide crosslinks between PG strands, presumably to allow for insertion of new
90 PG material during cell elongation (18-21). To ensure structural integrity, EP-mediated
91 cell wall cleavage and Rod- and/or aPBP-mediated resynthesis should logically be
92 tightly coordinated, and this has indeed been demonstrated for cell elongation in Gram-
93 positive bacteria (22-25). When the putative coordination is perturbed (*e.g.*, after
94 exposure to a cell wall synthesis inhibitor), PG structural integrity often catastrophically
95 fails and cells die (26); this is one of the reasons why cell wall synthesis inhibitors (e.g.,
96 the β-lactams) rank highly among our most powerful antimicrobials (27). EPs in

particular are a double-edged sword as they can both promote cell wall synthesis (28) and play major roles in cell wall cleavage after beta lactam exposure (29, 30). However, how EPs are regulated has only begun to be unravelled (31-34), and, at least in Gram-negative bacteria, we lack a complete understanding of how EP cleavage activity relates to PG synthesis by the two distinct cell wall synthase complexes.

Several models have been advanced to explain coordination of synthesis and degradation, with a prominent model being a “make before break” mechanism, where a nascent PG layer scaffold is elaborated parallel to an existing one, followed by cleavage of the old material that has been relieved of its critical structural function through this nascent PG load-bearing stabilizer (35, 36). Alternatively, PG might be able to sustain several cleavage events without experiencing catastrophic structural failure, obviating the need for any coordination between synthesis and degradation for as long as the Rod system and/or aPBPs are efficient enough in recognizing gaps in PG, *e.g.*, through interaction with their cognate OM-localized activators in case of the aPBPs (a “break before make” model).

Here, we show that in the cholera pathogen *Vibrio cholerae,* EP activity is not required for cell wall synthesis *per se*. During EP insufficiency, growth and PG accumulation continue in the presence of Rod system inhibitors but abruptly stop upon inhibition of aPBPs. However, the Rod system continues directed motion for extended periods of EP depletion. Lastly, a heterologously expressed EP can fully complement growth and morphology of an EP-deficient *V. cholerae* strain. Our data suggest that aPBPs do not

require wild-type levels of crosslink cleavage for PG incorporation (and consequently cell expansion), and that EP activity is required for the Rod system to contribute substantially to proper rod-shaped growth. Our cross-species complementation experiments intriguingly raise the possibility that direct co-ordination between EPs and cell wall synthases might not be necessary at all, at least under standard laboratory growth conditions.

Results

Cell wall incorporation and mass increase continue during endopeptidase insufficiency in V. cholerae

Endopeptidase depletion was previously shown to preclude insertion of new cell wall material in *E. coli,* resulting in rapid cell lysis (21). In contrast, we have noticed during EP depletion experiments with *Vibrio cholerae* that the cholera pathogen did not lyse, even in the absence of all 6 of its major D,D-EPs. This Δ6 endo strain (Δ*shyA* Δ*shyB* Δ*shyC* Δ*vc1537* Δ*vc0843,* Δ*vca1043* P_{IPTG}:*shyA*), has the remaining, conditionally essential EP ShyA under control of an IPTG-inducible promoter and is thus suitable for depletion experiments. Upon growing the Δ6 endo strain in the absence of inducer (reducing ShyA to less than 10 % of initial levels after ~ 2h, **Fig. S1**), mass increase (measured by OD_{600}) continued at a rate similar to when *shyA* expression was induced by IPTG (**Fig. 1A**). When plated on solid medium containing inducer at various timepoints after initiation of depletion, however, we observed a slight decrease in cfu/mL (**Fig. S2A**). Thus, the ability to recover and form colonies on a plate decreases during EP insufficiency. Additionally deleting the genes encoding PBP4, PBP7 and VC1269

(which have predicted EP activity but are, based on *E. coli,* not required for growth and cell elongation (37, 38)) did not appreciably affect mass increase (except for a slight decrease in final yield after 6 h; for an unknown reason, the strain also exhibitied a more pronounced drop in cfu/mL than Δ6 endo) (**Fig. S2B**), demonstrating that the mass increase phenotype did not simply reflect the ability of these putative EPs to substitute for ShyA.

We have previously shown that EP depletion in the Δ6 endo strain results in a dramatic increase in cell diameter and ultimately the generation of giant, bulky and contorted cells (34). Here, we probed the impact of endopeptidase insufficiency on PG composition and incorporation. PG architecture analysis revealed, as expected, that Δ6 accumulated a higher percentage of PG crosslinks after ShyA depletion (38.5%) compared to when ShyA is present (29.3 %), presumably due to the lack of EP cleavage activity (**Fig. S2C-D**). The analysis further revealed a 65% increase in trimer formation, as well as a 32% increase in the amount of anhydro residues upon ShyA depletion (**Fig. S2C-D**). Overall, the increase in crosslinking provides additional evidence that functional EP availability was highly limited under our depletion conditions. We next asked whether these enlarged cells elaborated a wild-type PG cell wall. To probe this, we cultured Δ6 endo in the presence of a fluorescent D-amino acid-derivative (HADA) as a cell wall stain (39). Addition of HADA to ShyA-replete Δ6 endo cells resulted in an even distribution of staining along the cell wall (**Fig. 1B**), as expected from wild-type cell wall synthesis. In contrast, depleting ShyA resulted in a strikingly different pattern, where large patches of HADA-reactive material accumulated

throughout the cell, indicative of substantial cell wall synthesis. In principle, these patches could be a remnant of incompletely-degraded cell wall material synthesized before ShyA was completely depleted, or they could reflect the activity of L,D-transpeptidases (which are able to incorporate HADA into the cell wall independent of cell wall synthesis (39, 40)). We thus repeated the staining experiment in a Δ6 endo strain lacking L,D-transpeptidases (Δ*ldtA* Δ*ldtB*). Following a 2 h depletion we added HADA for an additional hour; this still revealed an accumulation of PG patches (**Fig. 2D**), strongly suggesting that PG synthesis and incorporation continues during endopeptidase insufficiency, albeit in an aberrant, non-directional way. Quantification of PG confirmed and expanded these observations – after 2 h of ShyA depletion, cells accumulated ~18-fold more PG than ShyA-replete cells (when normalized to OD_{600}) (**Fig. 1C**). Since these cells did not divide (**Fig. S2A**), PG accumulation was not correlated with an increase in cell numbers, but suggested a buildup of cell wall in the invididual, drastically enlarged ShyA-depleted cells. Consistent with a higher cell wall content, ShyA-depleted Δ6 endo cells were almost 10-fold more resistant to osmotic shock treatment (**Fig. 1D**). Thus, ShyA-depleted Δ6 endo cells not only incorporate PG, but retain higher levels of PG than the WT, possibly reflecting the lack of EP-initiated turnover processes. Similar observations have been made in autolysin-inactivated *B. subtilis,* a Gram-positive bacterium (25, 41, 42). While we cannot rule out that residual ShyA remains in the cell following depletion (at levels too low to detect above background of the non-specific band we observed via Western Blot in the same size range as ShyA, **Fig. S1**), we can at a minimum conclude that *wild-type levels* of EPs are not necessary to facilitate mass increase and incorporation of PG *per se*, but are

essential for cell division and likely key for the proper, directional integration of PG into the sacculus of *V. cholerae*.

Cell wall incorporation and mass increase in EP-deficient cells rely primarily on aPBPs

We next addressed whether EP insufficiency affected the two cell wall synthesis machines, the Rod system and the aPBPs, differentially. To this end, we repeated our Δ6 endo depletion experiment in the presence of MP265 (an inhibitor of MreB (43)) or moenomycin (an aPBP glycosyltransferase inhibitor (44)). When ShyA was expressed, mass increase proceeded at similar rates for both antibiotic treatments and the untreated control (**Fig. 2A)**, while cfu/mL plateaued (moenomycin at 10 μg□ml^{-1}, 8 x MIC) or decreased 10- 20-fold (MP265 at 200 μM, 15 x MIC) in the presence of antibiotic (**Fig. S3A**). The continued OD_{600} increase upon antibiotic exposure is consistent with our previous observations that *V. cholerae* (as well as many clinically significant Gram-negative pathogens) is remarkably tolerant to inhibitors of cell wall synthesis. Exposure to such agents causes *V. cholerae* to form cell wall-deficient spheroplasts (in the presence of aPBP inhibitors) or spheroid cells containing cell wall material (in the presence of MreB inhibitors) (30, 45). Importantly, both sphere cell types continue to increase in mass (30, 45), but fail to divide. Thus, OD_{600} continues to increase while cfu/mL stagnates or declines.

Upon ShyA depletion, mass increase in the presence of MP265 continued at a similar rate compared to ShyA-replete conditions, and we observed substantial HADA

incorporation (**Fig. 2B, Fig. 2D**), suggesting that the Rod system was not absolutely required for PG synthesis during EP insufficiency. MP265-treated cells under ShyA depletion conditions qualitatively exhibited a rounder morphology than those in the untreated control, but were intact and enlarged (**Fig. 2C)**. Importantly, the mass increase, HADA incorporation, and morphological aberrations were recapitulated when another Rod system inhibitor, the bPBP2 inhibitor mecillinam, was used (**Fig. S3C-F**).

In striking contrast to Rod system inhibition, aPBP inhibition via moenomycin exposure completely abrogated growth (measured by OD_{600}) of ShyA-depleted Δ6 endo cells (**Fig. 2B**). This coincided with accumulation of small cells and debris (indicative of lysis), notably without strong HADA incorporation (**Fig. 2C-D**). In addition, cell viability declined rapidly in early stages (consistent with our previous observations (30)), though ultimately exhibited levels of survival similar to untreated or MP265-treated, ShyA-depleted Δ6 endo cells (**Fig. S3A-B**). In summary, our data suggest that during EP-insufficiency, the aPBPs contribute to both mass increase and sustained PG incorporation, while the Rod system is not absolutely required.

MreB movement continues in EP-insufficient cells

The Rod-system, in conjunction with the actin homolog MreB, deposits new cell wall material during cell elongation while performing a rotational movement around the cell, apparently driven by aPBP-independent cell wall synthesis (46-48). Since the Rod system did not appear to contribute to PG synthesis during EP insufficiency, we asked whether EP depletion resulted in immobile Rod-complexes, similar to what has been

observed during inhibition of cell wall synthesis (47). We constructed a functional (**Fig. S4**) mreBmsfGFP sandwich fusion in a Δ6 endo background and measured mreBmsfGFP velocity using epifluorescence and Total Internal Reflection Fluorescence (TIRF) microscopy. As a positive control, we confirmed that MP265 stopped MreB movement (**Fig. 3B**), as expected from what has been reported in *E. coli*. Mean square displacement values indicated mixed populations of diffusive MreB particles and those exhibiting directed motion under both ShyA replete and depleted conditions (**Fig. S5**). Interestingly, MreB movement continued even after 3 h of ShyA depletion (**Fig. 3D**), albeit at reduced velocity (decreasing from ~70 nm/s to ~ 40 nm/s) compared to ShyA-replete conditions (**Fig. 3C**). Our estimates of MreB velocity under ShyA replete conditions were higher than what has been reported previously for other bacteria (55 nm/s for *B. subtilis* (49) and 10 nm/s for *E. coli* (47)), perhaps reflecting species-specific differences or different properties of our sandwich fusion. Interestingly, the average size and number of MreB clusters also increased under ShyA depletion conditions (**Fig. 3E-G**), suggesting that EP depletion might affect Rod complex assembly dynamics. We conclude that similar to what has been observed in *B. subtilis* (22), EP insufficiency does not result in immediate inactivation of the Rod system, but changes its velocity and potentially the stoichiometry of its assembly.

Complementation of EP-insufficiency in* V. cholerae *by expression of heterologous EPs

So far, our results suggested that during EP insufficiency, aPBPs continue to synthesize PG and the Rod system may remain functional, yet does not insert substantial amounts

of new PG material into the sacculus. This might suggest that the Rod system requires a physical association with one or more EPs for insertion of nascent PG material. Alternatively, EPs might catalyze PG insertion independently, *e.g.*, through recognition of intrinsic PG substrate cues. To gain a better understanding of the necessity for a physical interaction, we conducted cross-species complementation experiments using an EP from *Neisseria gonorrhoeae* (henceforth "$MepM_{Ngo}$"). This distantly related EP (a BLAST alignment indicated 29 % identity between $MepM_{Ngo}$ and ShyA, **Fig. S6**), when heterologously expressed, is unlikely to interact with any native *V. cholerae* enzymes, and should thus allow us to isolate their EP activity from the interaction networks they might be embedded in. We expressed arabinose-inducible $MepM_{Ngo}$ in Δ6 endo and measured differential growth in the presence of IPTG (ShyA expression) vs. arabinose ($MepM_{Ngo}$). We found that wild-type $MepM_{Ngo}$ was unable to rescue growth of a Δ6 endo during ShyA depletion conditions (**Fig. 4A**). However, we recently demonstrated that EPs from diverse organisms (including *E. coli* and *N. gonorrhoeae*) are produced predominantly in an inactive form due to the inhibitory function of their domain 1 and likely activated *in vivo* by an unknown mechanism (34). Heterologously expressed enzymes may not be subject to this activation pathway in *V. cholerae* (especially if the activator is a protein) and we thus instead expressed EP mutant versions with their inhibitory domain 1 deleted, rendering them constitutively active, and provided a signal sequence (ss) to ensure export to the periplasm. Surprisingly, $ssMepM_{Ngo}^{\Delta Dom1}$ fully complemented growth of the Δ6 endo strain to a similar degree as the native ShyA (**Fig. 4A**). Visual inspection of Δ6 cells relying on heterologous expression for growth (ara+ condition), revealed that complementation with $ssMepM_{Ngo}^{\Delta Dom1}$ (but not its active site

mutant derivative H373A) promoted both growth (**Fig. 4A**) and the generation of rod-shaped cells (**Fig. 4B**). We sought to confirm that this apparent complementation of rod shape was still dependent on $MepM_{Ngo}^{\Delta Dom1}$ (rather than a mutation derepressing *shyA* in Δ6 endo). Thus, we plated all strains on agar containing IPTG, arabinose, or no inducer at the end of the experiments where we visualized cells relying on $MepM_{Ngo}^{\Delta Dom1}$ for growth. All strains had the same low level of spontaneous supressors able to grow in the absence of inducer (**Fig. S7**), confirming that the majority of the rod-shaped cells observed when only $MepM_{Ngo}^{\Delta Dom1}$ was expressed are not suppressors. Interestingly, we found that heterologous expression of activated MepM from *E. coli* ($ssMepM_{Ngo}^{\Delta Dom1}$) was able to restore growth, but not rod-shape, to Δ6 endo *V. cholerae* (**Fig. S8**). Thus, for an unknown reason, intrinsic properties of specific EPs (or rather these mutant derivatives) define their ability to complement of Δ6 endo cell shape. In summary, these data demonstrate that heterologous expression of an activated EP can be sufficient to restore both growth and (in the case of the *N. gonorrhoeae* EP) proper cell shape to Δ6 endo cells.

Discussion

Bacteria must maintain a careful balance between cell wall cleavage and synthesis to promote cell elongation/division, but the exact relationship between the two cell wall synthases (Rod system vs. aPBPs) and cell wall hydrolases (*e.g.*, endopeptidases) is poorly understood, at least in Gram-negative bacteria. Here, we have used EP depletion and chemical inactivation experiments to dissect the interplay between cell wall cleavage and synthesis in the cholera pathogen *V. cholerae.* Our key observation is that

in *V. cholerae,* cell wall synthesis and cell expansion (but not cell division) continue upon EP depletion. This poses an apparent contradiction to data obtained in *E. coli,* where cell wall incorporation was drastically reduced after EP depletion and cells started to lyse (21). While ostensibly fundamental aspects of the coordination between cell wall synthesis and cleavage may simply not be as well-conserved as one might expect, these observations might also reflect species-specific differences in EP-independent cell wall turnover rates, and not necessarily the consequences of EP depletion *per se*. It is possible that lysis under EP-insufficient conditions in *E. coli* reflects generally higher PG degradation rates (*E. coli*, for example encodes three amidases (50), while *V. cholerae* possesses only one (51)). This would mask the underlying continued incorporation of new cell wall material in the absence of EPs. Importantly, EP depletion in *E. coli* did result in a cell volume increase prior to lysis (21), also supporting at least a transient continuation of PG synthesis during EP insufficiency in this species.

Cell wall expansion during EP-insufficiency was surprising, since presumably any form of cell wall synthesis that promotes the degree of cell expansion we observed in EP-deficient *V. cholerae* should require some form of cleavage, likely catalyzed by other autolysins. The incisions resulting from such cleavage, and/or the autolysin(s) involved appear to be of limited utility to the Rod-system, but can be exploited by the aPBPs. This suggests that aPBPs are more versatile in recognizing a variety of cell wall cuts (independent of an actual physical connection with EPs), while the Rod system primarily relies on either EP-mediated cleavage, or a physical association with EPs (see a more

detailed discussion below) for substantial PG incorporation and cell expansion. These interpretations are in line with some old and several recent proposals based on data from *E. coli* that aPBPs and SEDS have separate (yet perhaps overlapping) functions during cell elongation (14, 52, 53). It has also been shown that, in *E. coli,* upregulated EP activity promotes aPBP function, likely indirectly through the creation of PG incisions that allow for an interaction between aPBPs and their OM-localized activators (28). Thus, EP cleavage may not be strictly necessary for, but can promote, aPBP activity. It is possible that under EP-insufficient conditions, the lytic transglycosylases (the other major group of cell wall cleavage enzymes that cut the polysaccharide backbone of PG (54)) create large open areas in PG that can be recognized, and patched, by aPBPs; LTG activity would be consistent with the increase in anhydro “caps” we observe in ShyA-depleted Δ6 endo PG from *V. cholerae*.

The observation (consistent with what has been shown in *B. subtilis* (22)) that MreB continues directed movement at least for some time during EP insufficiency suggests that the Rod system does not actually require wild-type EP activity for assembly and for RodA’s glycosyltransferase activity (which likely drives MreB movement). Similar to what has been proposed for *B. subtilis,* it is tempting to speculate that *V. cholerae* may use a “make-before-break” model as proposed by Höltje/Koch (35, 36) for cell elongation via the Rod system. In this model, the Rod system creates a second layer of PG that is incorporated via EPs during or after synthesis. Generation of this second layer could at first proceed independently of wild-type EP activity, but incorporation into the growing sacculus would require crosslink cleavage.

As mentioned above, our data suggest that to contribute substantially to cell expansion and PG incorporation, the Rod system requires EP activity, either through physical association or recognition of EP cut sites in PG. Our cross-species complementation experiments with an activated *N. gonorrhoeae* EP suggest that a physical association might not be strictly necessary, unless the heterologously expressed (and truncated) enzyme does somehow directly interact with the *V. cholera*e Rod system. We thus consider a model plausible where rather than (or in addition to) co-ordinating with cell wall synthases directly, EPs can somehow specifically recognize and preferentially cleave old PG that is adjacent to nascent PG. Though highly speculative, our observation that the corresponding *E. coli* homolog does not complement cell shape might reflect different levels of activity – since EPs can promote aPBP activation (at least in *E. coli*) (28), overexpression of a more active EP might divert PG precursor flux away from the Rod system towards aPBPs to a higher degree than the *N. gonorrhoeae* enzyme, incapacitating a cell's ability to elaborate a rod shape.

An important caveat to the complementation experiments, is that the Δ6 endo strain still maintains a copy of *shyA* under IPTG control. While the lac promoter is tightly repressed in the absence of inducer, a small number of molecules under its control might still be produced (55). ShyA is produced predominantly as an inactive precursor and the signal for activation is unkown (34). It is conceivable that complementation with a heterologously expressed EP might somehow enhance activation of this leaky

372 background of ShyA molecules*, e.g.* if there is a positive feedback loop between cell
373 wall cleavage and native EP activation.
374
375 Taken together, our data suggest that two main cell wall synthases, the aPBPs and the
376 Rod system have differential relationships with autolysins, and especially
377 endopeptidases. As such, our data provide additional support for the emerging theme of
378 at least partially differential roles of the aPBPs and the Rod system during cell
379 elongation.
380
381

382 ## Acknowledgements

383 This work was supported by the National Institutes of Health/NIGMS through R01
384 GM130971 to TD. Research in the Cava lab is supported by MIMS, the Knut and Alice
385 Wallenberg Foundation (KAW), the Swedish Research Council and the Kempe
386 Foundation. Research in the VanNieuwenhze lab is supported by the NIH through R01
387 GM113172 and R35 GM136365. TIRF imaging was supported by grant NSF 1428922
388 to the BRC imaging facility at Cornell.
389
390

391 ## Materials and Methods

392 **Bacterial growth conditions.**

393 Cells were grown by shaking (200 rpm) at 37^{o}C in 5 mL of LB in borosilicate glass tubes
394 (14 mL capacity) unless otherwise indicated. Where appropriate, antibiotics were used

as the following concentrations: streptomycin, 200□µg□ml^{-1}; ampicillin, 100□µg□ml^{-1}; chloramphenicol, 5□µg□ml^{-1}; moenomycin, 10 µg□ml^{-1}; MP265, 300 µM; and mecillinam,10 µg□ml^{-1}. IPTG (200□µM) and arabinose (0.2%) were added for induction of P_{iptg} and P_{ara} promoters, respectively.

Plasmid and strain construction.

All bacterial strains and oligonucleotides used in this study are summarized in **Table S1**. All *Vibrio cholerae* strains are derivatives of El Tor strains N16961 (56) or E7946 (57), the latter was used for chitin-induced transformation.

Δ6 endo construction is reported elsewhere (30). Other strains were constructed by chitin-induced transformation of linear PCR products as described in (58). A chloramphenicol (*chl*) resistance cassette insertion into the gene *vc1807* (a well-established neutral locus) was used as the primary selector. The transforming fragment for vc1807::chl was constructed by amplifying upstream and downstream homology regions using primers PD079/PD097 and PD098/PD082, respectively. The *chl* gene coding for chloramphenicol acetyl transferase was amplified from pBAD33 (59) with primers PD095/PD096 and fused with the flanking homologies of vc1807 via isothermal assembly. For antibiotic resistance gene swapping, a vc1807::trim allele was also produced by amplifying upstream (using primers TDP597/598) and downstream (primers TDP601/602) homologies of vc1807 and fusing them with a trimR cassette amplified from *V. cholerae* Haiti (60) (primers TDP599/600) using SOE PCR with primers TDP603/604.

418

419 To construct a functional MreB-msfGFP-MreB sandwich fusion, upstream (primers
420 PD056/PD074) and downstream (primers PD071/PD057) homologies were amplified
421 from the *V. choerae* genome and fused via isothermal assembly with msfGFP (amplified
422 with primers PD054/PD055). Analogous to a published *E. coli* MreB-msfGFP sandwich
423 fusion (47), we replaced glycine 228 of MreB with this msfGFP. To enhance the
424 probability of success of finding a functional fusion, we used semi-degenerate primers
425 to generate a library of possible linker sequences. Flanking homologies, MreB and
426 msfGFP were first fused using isothermal assembly (61) and then amplified using
427 nesting primers PD104/PD105. The resulting upstream-MreB-linker-msfGFP-linker-
428 MreB-downstream PCR fragments were transformed into E7946 using chitin
429 transformation with vc1807::chl as the primary selector. 96 colonies were tested for
430 growth rate and clone M2C was chosen for further experiment due to its wild-type
431 growth behavior. The linkers of this fusion construct were sequenced (coding for
432 DGVGG upstream of msfGFP and GTPIP downstream).

433

434 Δ8 was constructed by transforming endopeptidase deletion PCR products into a
435 parental mreB::mreBmsfGFP ΔlacZ::P_{IPTG}:*shyA* strain. Deletion scars were amplified
436 from Δ6 endo and introduced in two steps into this parental background via chitin
437 transformation. The following primers were used to amplify the EP deletion fragments:
438 *shyA* (TDP577/578), *shyC* (TDP581/582), *shyB* (TDP579/580), *vc1537* (TDP583/584),
439 *vc0843* (tagE1) (TDP587/588), *vca1043* (tagE2) (TDP585/586). PBP4 and PBP7
440 deletions were introduced into Δ6 endo by amplifying PCR fragments with upstream and

441 downstream homologies fused by a linker for chitin-mediated transformation. PBP4
442 upstream homology (TDP680/TDP681) and downstream homology (TDP682/TDP683)
443 were fused using SOE PCR with nesting primers (TDP691/TDP692). PBP7 upstream
444 homology (TDP676/TDP677) and downstream homology (TDP678/TDP679) were fused
445 using SOE PCR with nesting primers (TDP693/TDP694). For the Δ*ldtA* Δ*ldtB* strain,
446 deletion scars were amplified from strain FC670 (40) using primers TDP654/55
447 (*vc1268)* and TDP656/57 (*vca0058),* respectively, and transformed into Δ6 endo using
448 chitin transformation as described above.
449
450 Δ8 exhibited a very low transformation efficiency and we thus introduced the Δ*vc1269*
451 deletion using homologous recombination with a suicide plasmid pCVD442 as
452 described (62). In brief, upstream and downstream homologies of vc1269 were
453 amplified using primers TD810/TD811 and TD812/TD813. These fragments were
454 cloned into Xba1-digested pCVD442 using isothermal assembly. pCVD442(Δvc1269)
455 was then introduced into Δ8 endo via biparental mating (using SM10 as a donor strain)
456 by mixing 10 µL of each donor and recipient, followed by 6 h incubation at 37 ˚C,
457 followed by selection for single crossover strains and against the donor strain by plating
458 on LB plates containing carbenicillin (100 µg□ml^{-1}), streptomycin (200 µg□ml^{-1}) and
459 IPTG (200 µM). A single colony from the first crossover plate was then picked and
460 streaked out on a plate containing sucrose (10 %), streptomycin (200 µg□ml^{-1}) and
461 IPTG (200 µM). This plate was incubated at ambient temperature for 3 days, after which
462 16 colonies were tested for the correct knockout construct using vc1269 flanking
463 primers TD814/TD815.

All plasmids were built using isothermal assembly (61). Genes were cloned into pBADmob (a mobile pBAD33 derivative) using the following primer pairs: $MepM_{Ngo}$, TDP1365/TDP1367, $ssMepM_{Ngo}$, SM861/SM862; $ssMepMNgo^{\Delta dom1}$, SM859/SM860; $MepM_{ECO}$, TDP1342/TDP1340; and $MepM_{ECO}^{\Delta dom1}$, TDP1341/TDP1340. The H373A point mutation was introduced into pBAD plasmids carrying NGO1686 derivatives via Q5 site-directed mutagenesis (NEB, Ipswitch, MA, cat #E0554S) with primer pair TDP1652/TDP1653. Plasmids were conjugated into *V. cholerae* using donor *E. coli* strains (SM10 lamda pir or MFD lamda pir).

Phase contrast microscopy and HADA staining

Cells were harvested (2 min at 12,000 rpm), spotted on a 0.8% agarose pad containing PBS and imaged on a Leica Dmi8 inverted microscope. For HADA experiments, Δ6 endo cells were grown in the presence of 50 µM HADA (3-[[(7-Hydroxy-2-oxo-2*H*-1-benzopyran-3-yl)carbonyl]amino]-D-alanine hydrocholoride), washed once by pelleting cells (2 min at 12,000 rpm) and resuspending in fresh LB. HADA stain was imaged in the DAPI channel (395 nm [excitation]/460 [emission]) at 1 s exposure.

Endopeptidase depletion experiments

EP depletion strains were grown overnight in LB broth containing 200 µM IPTG. The next day, cells were washed 2x by pelleting (2 min at 12,000 rpm) and resuspending in LB broth without inducer. Cells were then diluted 100-fold into fresh LB containing either

200 µM IPTG (ShyA +) or no inducer (ShyA -). Where indicated, antibiotics were used at 10 µg□ml^{-1} (moenomycin, mecillinam) or 200 µM (MP265).

Single particle tracking by TIRF imaging

The Δ8 endo mreB::mreBmsfGFP^{SW} strain with chromosomally expressed MreB-msfGFP was grown shaking at 37°C in LB medium supplemented with 100µM IPTG overnight. The saturated cells were diluted (1:100) into fresh LB in two groups (with 100µM IPTG for ShyA expression or without IPTG for ShyA depletion). After 2 hours of shaking (220 rpm) incubation at 37°C, cells were harvested and spotted on a 0.8% agarose pad containing M9 medium. Time-lapse TIRF imaging was performed on a Zeiss Elyra equipped with an inverted Axio Observer.Z1 microscope and a 100x 1.46 oil objective. The objective was heated at 37°C during image acquisition. The exposure time was 100 ms and inter-frame intervals were 2 s over a 2-min recording. The movement of MreB-msfGFP was analyzed using single particle tracking software ImageJ TrackMate (63) and MATLAB msdanalyzer (64).

The mean square displacements (MSD) of particle trajectories were calculated using the msdanalyzer package and the motion types were analyzed through log-log fitting (64). By setting the R^2 coefficient > 0.8, individual MSD curves were fitted and the values of anomalous diffusion coefficient (α) indicates that MreB particles exhibit a mix of dynamic behaviors (confined diffusion, $0.1 \leq \alpha < 0.9$; simple diffusion, $0.9 \leq \alpha < 1.1$; directed motion, $\alpha \geq 1.1$) (65).

Peptidoglycan analysis

PG samples were analyzed as described previously (66). Briefly, 50 mL cultures of Δ6 endo were grown to early/mid exponential phase with or without IPTG (200 µM) for 2h, harvested and boiled in 5% SDS for 1 h. Sacculi were repeatedly washed by ultracentrifugation (110,000 rpm, 10 min, 20ºC) with MilliQ water until SDS was totally removed. Samples were treated with 20 µg Proteinase K (1 h, 37 °C) for Braun's lipoprotein removal, and finally treated with muramidase (100 µg·ml^{-1}) for 16 hours at 37 ºC. Muramidase digestion was stopped by boiling and coagulated proteins were removed by centrifugation (14,000 rpm, 10 min). For sample reduction, the pH of the supernatants was adjusted to pH 8.5-9.0 with sodium borate buffer and sodium borohydride was added to a final concentration of 10 mg·ml^{-1}. After incubating for 30 min at room temperature, the samples pH was adjusted to pH 3.5 with orthophosphoric acid.

UPLC analyses of muropeptides were performed on a Waters UPLC system (Waters Corporation, USA) equipped with an ACQUITY UPLC BEH C18 Column, 130Å, 1.7 µm, 2.1 mm X 150 mm (Waters, USA) and a dual wavelength absorbance detector. Elution of muropeptides was detected at 204 nm. Muropeptides were separated at 45°C using a linear gradient from buffer A (formic acid 0.1% in water) to buffer B (formic acid 0.1% in acetonitrile) in an 18-minute run, with a 0.25 ml/min flow.

Relative total PG amount was calculated by comparison of the total intensities of the chromatograms (total area) from three biological replicas normalized to the same OD600 and extracted with the same volumes. Muropeptide identity was confirmed by MS/MS analysis, using a Xevo G2-XS QTof system (Waters Corporation, USA).

Quantification of muropeptides was based on their relative abundances (relative area of the corresponding peak) normalized to their molar ratio.

Western Blotting

Whole cell lysates (15 µg) were resolved by 10% SDS-PAGE and the proteins were transferred to a PVDF membrane using a semi-dry transfer system (iBlot 2, Invitrogen). The membrane was then blocked overnight with blocking solution containing 4% milk (dry milk dissolved in 20 mM Tris-HCl (pH 7.8), 150 mM NaCl, 0.1% Triton X-100). Next day, the membrane was incubated with anti-ShyA polyclonal antibody (1: 5,000, produced by Pocono Rabbit Farm & Laboratory, PA) for two hours and then washed twice with 1xTBST (20 mM Tris-HCl (pH7.8), 150 mM NaCl, 0.1% Triton X-100). The washed membranes were then incubated with anti-rabbit secondary antibody (1:15,000, Li-Cor cat# 926-32211) for 1 hour. Membranes were then washed three times with 1xTBST, scanned on an Odyssey CLx imaging device (LI-COR Biosciences) and visualized using Image Studio™ Lite Ver 5.2 software (Li-Cor) for signal quantification.

Figure legends

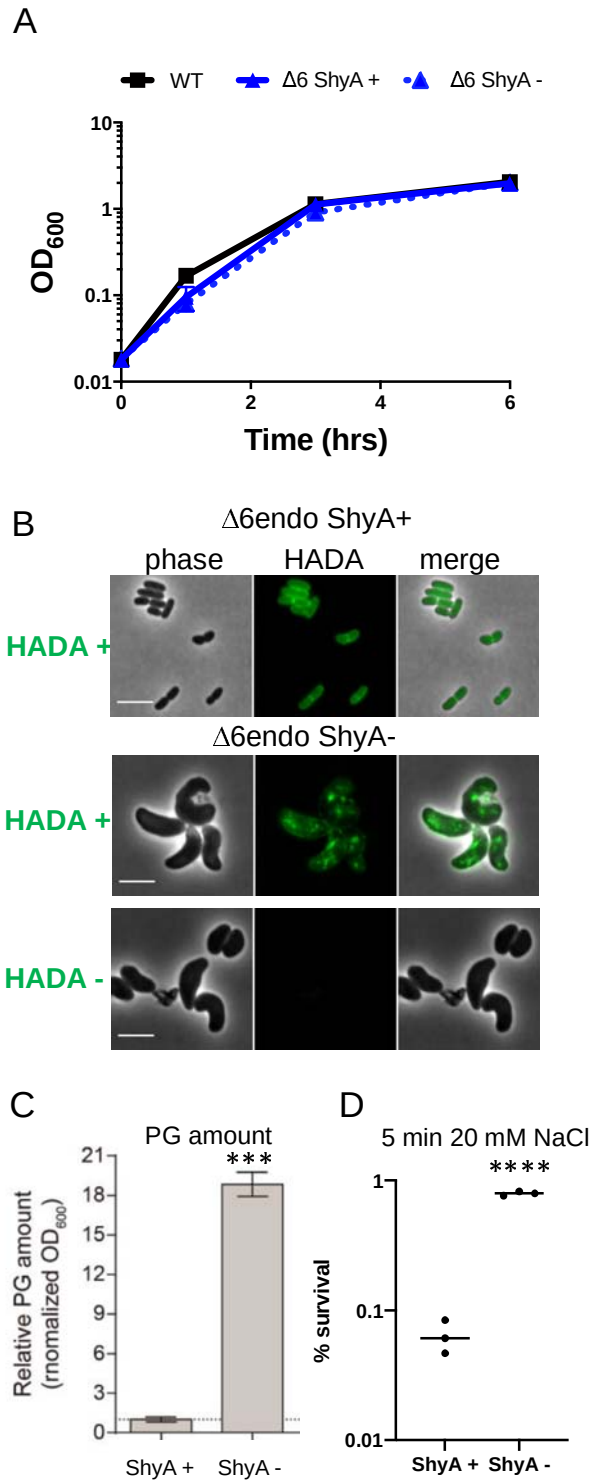

549

550

Figure 1. **Cell mass increase and cell wall incorporation continue during EP insufficiency. (A)** Overnight cultures of Δ6 endo (Δ*shyABC* Δ*vc1537* Δ*tagE1,2* P_{IPTG}:*shyA*) grown in the presence of IPTG (200 µM) were washed twice and diluted 100-fold into growth medium with (ShyA +) or without (ShyA -) IPTG. At the indicated time points, OD_{600} was measured. Data are mean of six biological replicates, error bars represent standard deviation. **(B)** Δ6 endo was treated as described in **(A)** in the presence of HADA (100 µM). After 3 h, cells were washed twice and then imaged. **(C)** Relative PG content of Δ6 endo was measured via UPLC analysis (see methods for details) after 2 hours of growth in the presence (ShyA +) or absence (ShyA -) of inducer. Error bars represent standard deviation of 3 biological replicates. **(D)** Cells were treated as described in (**A).** After 3 h of growth in the presence or absence of inducer, cells were pelleted and resuspended in 20 mM NaCl (osmotic shock treatment) for 5 min. Shock treatment was stopped by adding PBS to 180 mM. % survival is cfu/mL before treatment divided by cfu/mL after treatment. Raw data points of 3 biological replicates are shown. (**C-D**) Asterisks denote statistical difference via unpaired t-test (****, $p < 0.0001$; ***, $p < 0.001$, ** $p < 0.01$, * < 0.05). Scale bars, 5 µm

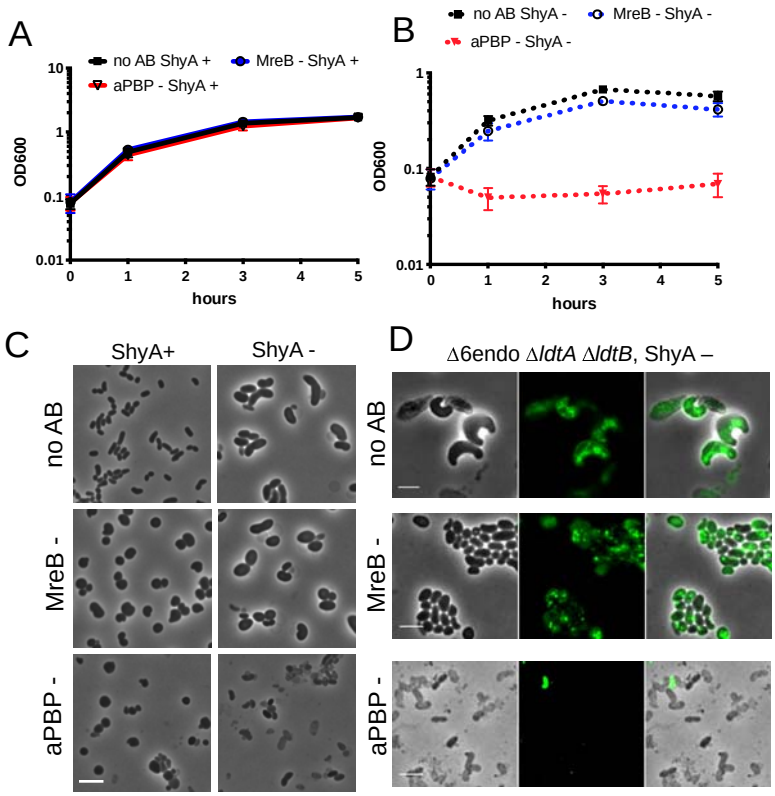

Figure 2. Cell mass increase and PG incorporation during EP insufficiency relies on aPBP activity. Δ6 endo grown overnight in IPTG (200 µM) was washed twice and diluted 100-fold into fresh medium containing either IPTG (ShyA+) **(A)** or no IPTG (ShyA -) (**B**) and either no antibiotic, the aPBP inhibitor moenomycin (aPBP -, 10 µg□ml^{-1}, 8x MIC) or the MreB inhibitor MP265 (MreB-, 300 µM, 15 x MIC). At the indicated time points, OD_{600} was measured; after 3 h of growth, cells were also imaged (**C**). Data are averages of six biological replicates, error bars represent standard deviation. Scale bar, 5 µm. (**D**) An overnight culture of Δ6 endo Δ*ldtA* Δ*ldtB* was diluted into medium without inducer. After 2 hours of ShyA depletion, HADA (100 µM) was added for another 1 hour. Cells were then washed twice and imaged. Antibiotics MP265 (MreB -) or moenomycin (aPBP -) were added for 1 h after the 2 h initial depletion, followed by 1 h addition of HADA. Scale bar, 5 µm.

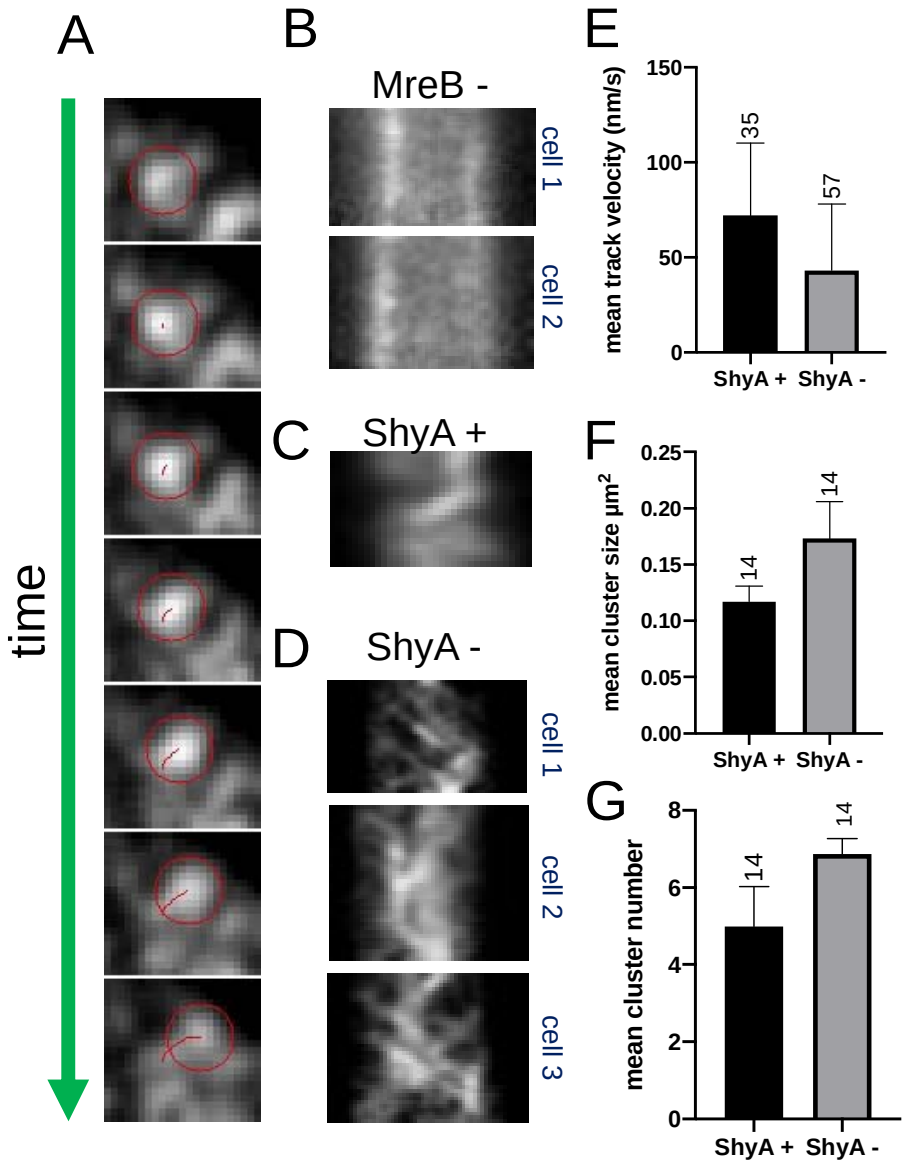

Figure 3. MreB movement continues during EP insufficiency.

Δ6 endo (**A-D**) or Δ8 endo (**E-G**) expressing an mreBmsfGFP^{SW} fusion from its native chromosomal locus was diluted from an overnight culture grown in the presence of IPTG into growth medium without inducer (ShyA -). After 3 hours, cells were imaged using epifluorescence microscopy (**A-D**) or TIRF (**E-G**). MreB movement was analyzed

588 using Fiji (TrackMate). A representative single moving MreB focus track (red circle) is
589 shown in (**A**) (frames are 2.5 s apart). Representative kymographs of MreB foci are
590 shown for cells grown (**B**) in the presence of the MreB inhibitor MP265 (MreB -), (**C**) in
591 the presence of inducer (ShyA +), or (**D**) in the absence of inducer (ShyA -). (**E-G**) TIRF
592 was used to assess MreB focus velocity, mean cluster size and mean cluster number.
593 Numbers above bar graphs represent the number of imaged cells, error bars represent
594 standard deviation. Differences between ShyA+ and ShyA – were significant for all three
595 graphs (t-test) at p = 0.017 (velocity), 0.021 (cluster size) and 0.028 (cluster number),
596 respectively.
597

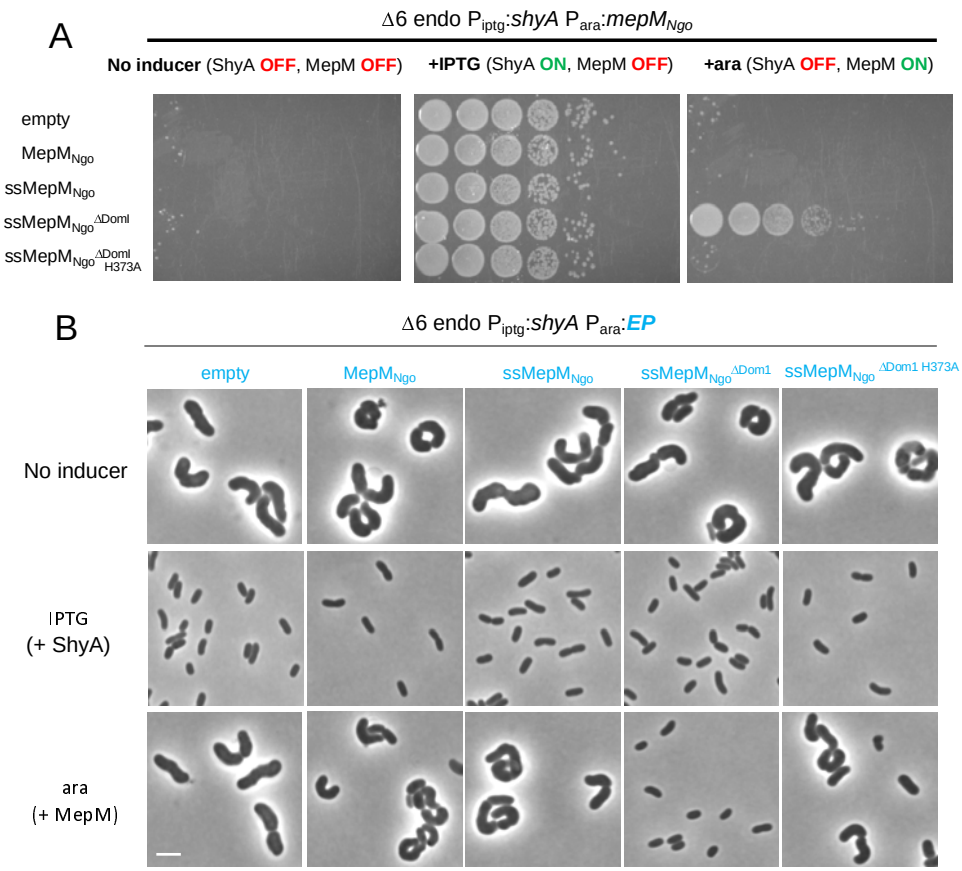

Figure 4. Cross-species complementation of Δ6 endo phenotypes with an EP from *Neisseria gonorrhoeae*.

(A-B) Δ6 endo was transformed with (arabinose-inducible) pBAD33 expressing an *N. gonorrhoeae* EP ($MepM_{Ngo}$). Derivatives of $MepM_{NGO}$ include an N-terminal dsbA signal sequence (ss), domain 1 truncation (ΔDom1)', or active site mutation (H373A). (**A**) Cells were washed and spot-plated on medium containing either no inducer, IPTG (200 µM) (chromsomal ShyA on), or arabinose (0.2%) (pBAD33-encoded $MepM_{NGO}$ on). Plates were incubated at 37 ˚C for 24 hours and then imaged. (**B**) Cells were diluted 100-fold and grown without inducer, with IPTG (+ ShyA), or with arabinose (+MepM) for 3 hours and then imaged. Scale bar, 5 µm.

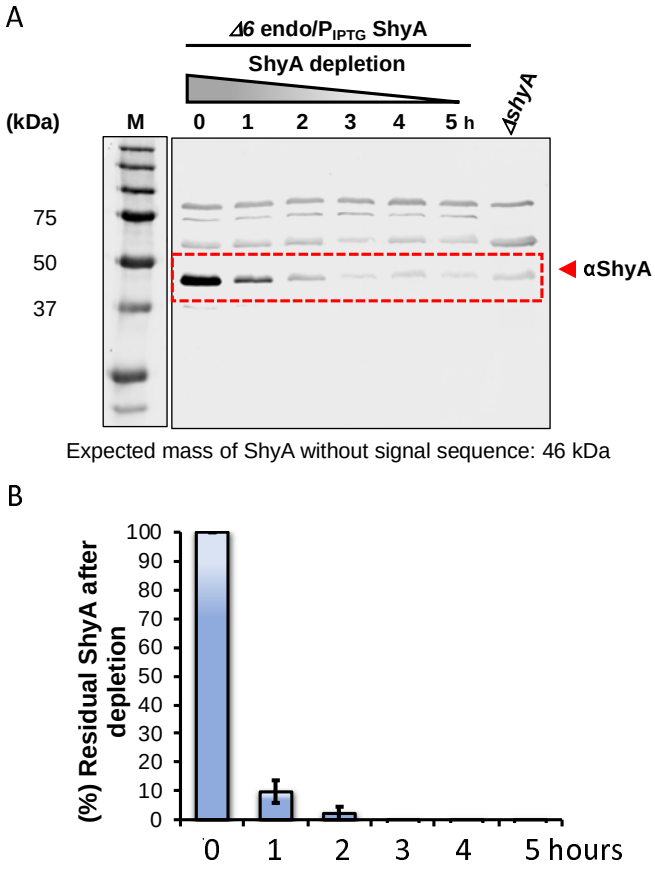

Figure S1. ShyA levels after depletion in Δ6 endopeptidase mutant. (A) Wild-type, Δ6 endo, and Δ*shyA* strains were grown overnight in LB broth containing 200 µM IPTG, then washed three times with fresh LB. Cells were then diluted 100-fold into 150 ml pre-warmed LB medium without IPTG for ShyA depletion. Samples were collected at indicated time points. For Western Blotting, cell extracts (adjusted to same protein concentration) were separated on 10% SDS-PAGE gels and subjected to Western Blot analysis using ShyA polyclonal antibody **(B)** ShyA band intensities were quantified (ImageJ) and the intensity value of the non-specific background band detected in the *ΔshyA* mutant was subtracted. Residual ShyA protein levels were normalized to non-depleted ShyA at 0 h (100%).

620

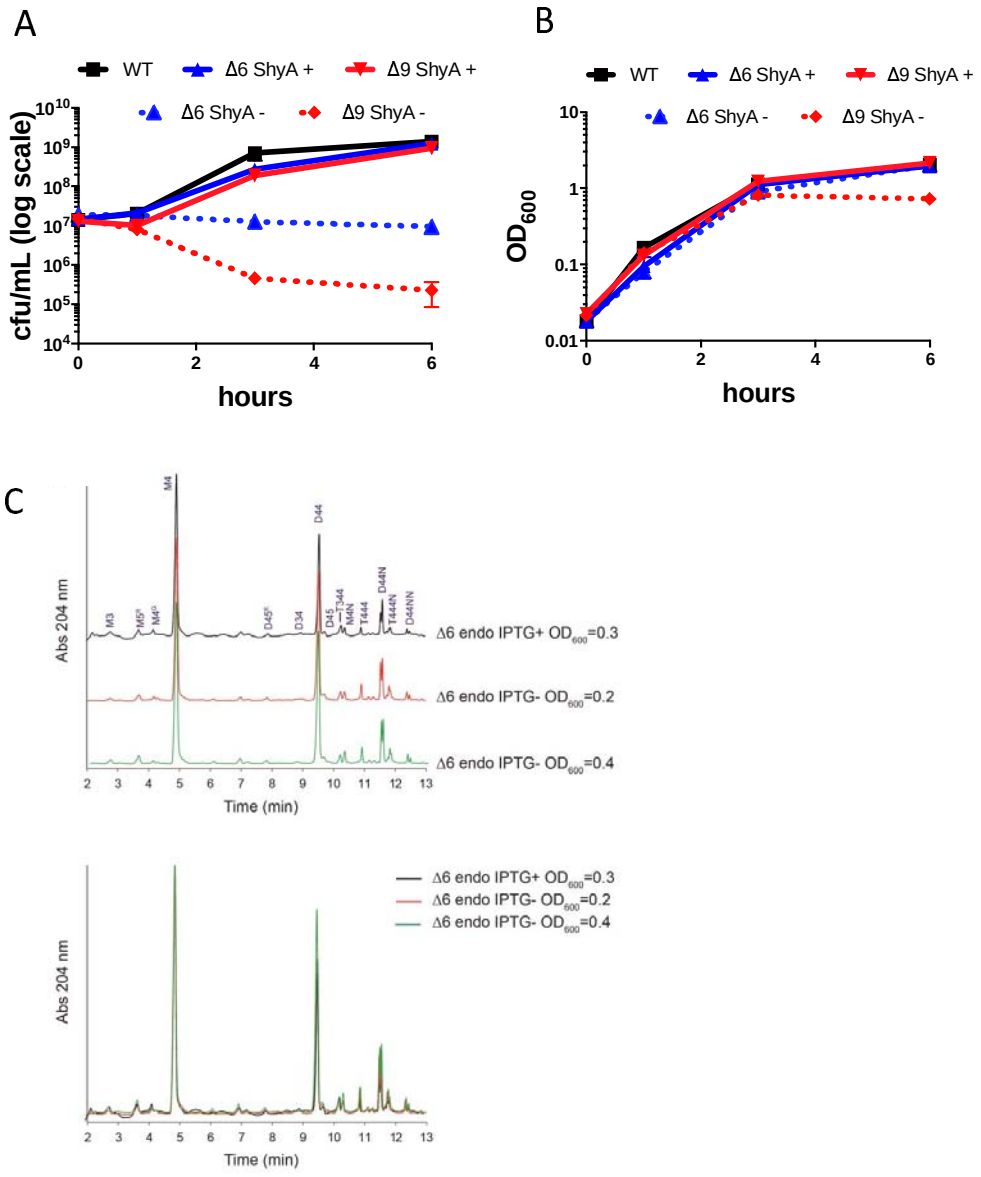

D

	Δ6endo ShyA+	Δ6endo ShyA -	% Change	P-value
Monomers	72.67	64.79	-10.8	***
Dimers	25.37	31.96	26.0	**
Trimers	1.97	3.24	65.1	**
Crosslink	29.30	38.45	31.3	****
Anhydro	7.79	10.24	31.5	***
Chain length	12.86	9.77	-24.0	**

621

Figure S2. Effects of EP depletion on growth, survival and PG composition.

N16961 Δ6 endo or E7946 Δ9 endo (mreB::mreBmsfGFP^{SW}) was grown overnight in IPTG (200 µM), washed twice, and diluted 100-fold into fresh medium with (ShyA +) or without (ShyA -) inducer. At the indicated time points, OD_{600} (**A**) was measured via spectrophotometry and cells were diluted serially onto LB IPTG (200 µM) plates to determine colony forming units per mL (**B**). Data are averages of 3 biological replicates, error bars represent standard deviation. (**C)** Chromatogram of PG composition of N16961 Δ6 endo cells harvested after 2 hours with (ShyA +) or without (ShyA -) IPTG (200 µM). **(D)** The table summarizes the relative molar abundance (%) of monomers, dimers, trimers shown in the chromatogram. Data regarding the % of crosslinkage (proportion of crosslinked peptide side chains, calculated on dimers and trimers content) is also included. Anhydro muropeptides (with a residue of (1-6 anhydro) N-acetyl muramic acid) are the terminal subunits of the sugar chains and hence used to calculate the chain length. Values are mean of three biological replicates. Percent change was calculated relative to the IPTG-treated sample and p-values were generated using a multiple comparisons t-test (****, $p < 0.0001$; ***, $p < 0.001$, ** $p < 0.01$, * < 0.05).

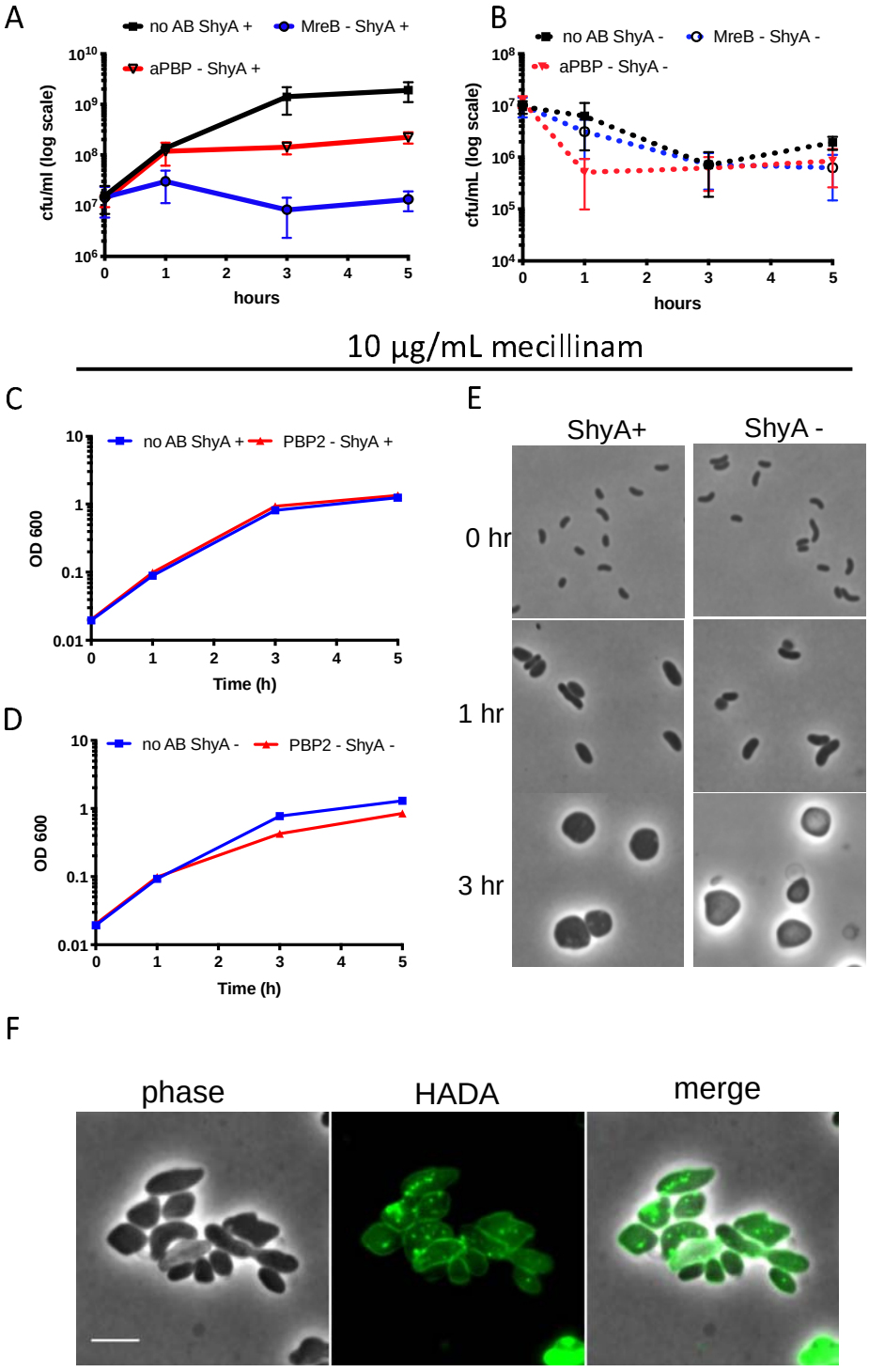

Figure S3. Mass increase during EP insufficiency relies on aPBPs, but not the Rod system.

641 Δ6 endo was grown overnight in IPTG (200 µM), washed twice, and diluted 100-fold into
642 fresh medium containing either IPTG (ShyA+) **(A)** or no IPTG (ShyA -) (**B**) and either no
643 antibiotic, the aPBP inhibitor moenomycin (aPBP -, 10 µg□ml^{-1}, 8x MIC) or the MreB
644 inhibitor MP265 (MreB -, 300 µM, 15 x MIC). At the indicated time points, cells were
645 diluted serially and spotted onto LB plates containing IPTG (200 µM). Data are
646 averages of six biological replicates, error bars represent standard deviation. (**C-E)** In a
647 similar experiment, Δ6 endo was treated with mecillinam (10 µg□ml^{-1}, 20x MIC). At the
648 indicated time points, OD_{600} (**C-D**) was measured via spectrophotometry and cells were
649 harvested and spotted on a 0.8% agarose pad containing PBS for phase contrast
650 microscopy (**E**). (**F**) The cell wall was stained using HADA as described for **Fig. 2D.**
651 Scale bar, 5 µm.
652

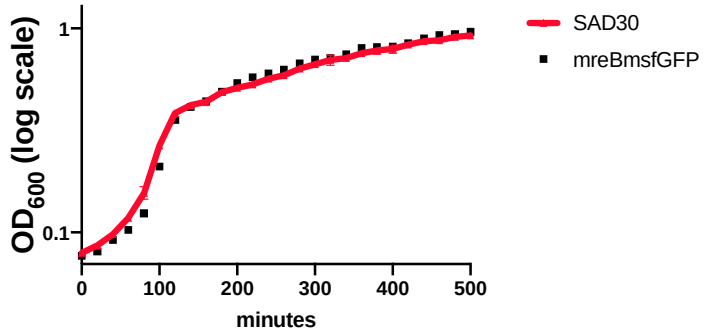

653

654 **Figure S4. Growth of the mreBmsfGFP strain compared to wild-type.**

655 Wild-type E7946 and mreBmsfGFP-containing derivative were grown overnight in LB.
656 Cells were diluted 1000-fold into fresh medium and 200-µl of each was loaded into a
657 100-well plate. Growth of each culture was monitored by optical density at 600 nm
658 (OD_{600}) in a Bioscreen C plate reader (Growth Curves America).

A

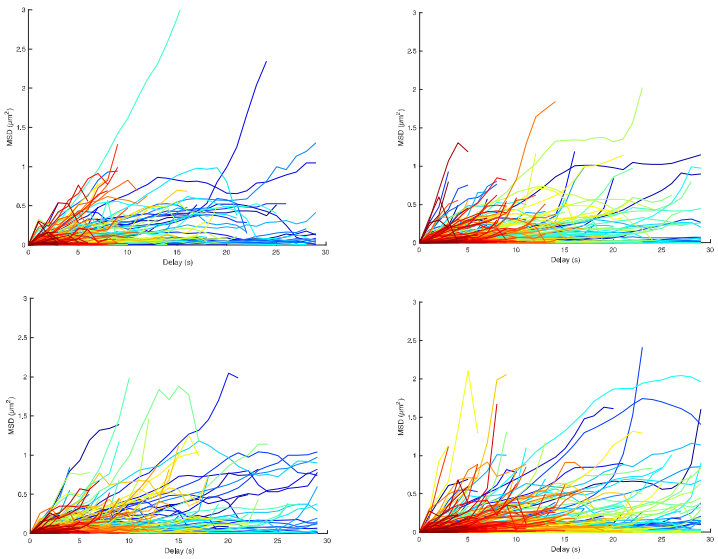

B

		IPTG +	ROI-1	ROI-3
	alpha			
confined motion	<0.9		34	42
simple diffusion	0.9≤ <1.1		10	19
directed motion	≥1.1		27	20
		total tracks (good fit)	71	81
		directed%	38.03%	24.69%

		IPTG-	ROI-1	ROI-2
	alpha			
confined motion	<0.9		55	72
simple diffusion	0.9≤ <1.1		36	47
directed motion	≥1.1		56	89
		total tracks (good fit)	147	208
		directed%	38.10%	42.79%

Figure [illegible] was grown with ([illegible] roscopy. **(A)** Exam[illegible] +/+ and IPTG- condit[illegible] cted motion.

Figure S6. ShyA and MepM$_{NGO}$ amino acid sequence alignment.

Amino acid sequences of *V. cholerae* endopeptidase ShyA (VCA0079) and *N. gonorrhoeae* ortholog MepM (NGO1686) were aligned in Clustal Omega (67). Numbers indicate the amino acid position relative to the start codon and alignment gaps are denoted with dashes. Symbols indicate the similarity of aligned residues: identical (*), strong similarity (:), and weak similarity (.).

672

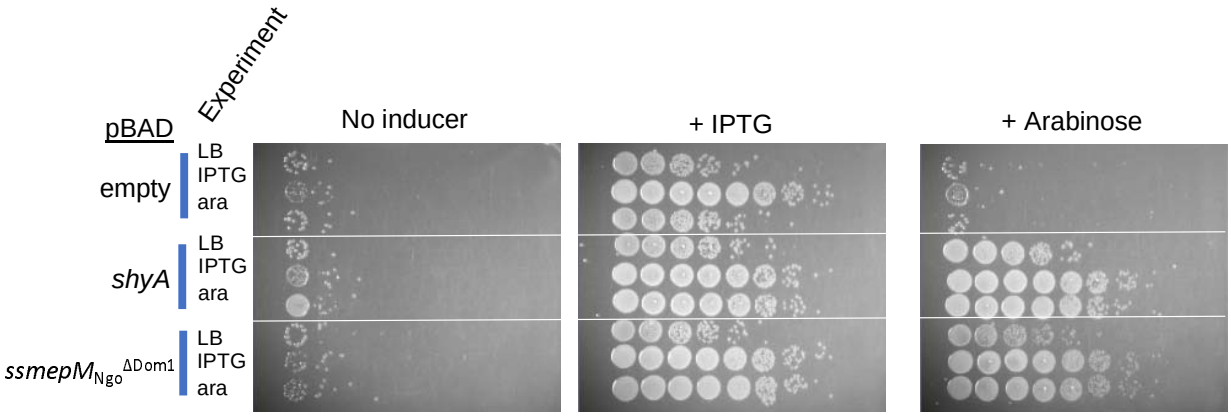

673

674 **Figure S7. Low suppressor background in Δ6 endo cells.**

675 Δ6 endo carrying pBAD33 (arabinose-inducible) expressing the indicated contructs
676 ("pBAD" column) were diluted into fresh medium containing either no inducer, IPTG or
677 arabinose (ara) and grown for 3 hours ("experiment" column). Cells were then spot-
678 plated on medium containing either IPTG (200 µM, ShyA expressed), arabinose (0.2 %,
679 $MepM_{Ngo}$ expressed) or no inducer. Plates were incubated at 37 ˚C for 24 hours and
680 then imaged.

681

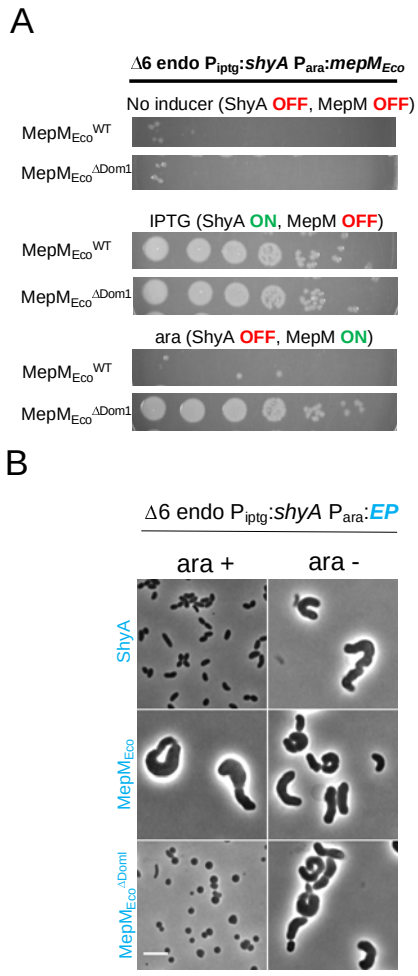

682

683 **Figure S8. Cross-species complementation of Δ6 endo phenotypes with an EP**
684 **from *Escherichia coli*.**

685 **(A)** Δ6 endo carrying pBAD33 (arabinose-inducible) encoding $MepM_{Eco}$ or its Δdomain 1
686 derivative, was diluted and spot-plated on medium containing either IPTG (200 µM,
687 ShyA expressed), arabinose (0.2 %, heterologous EP expressed) or no inducer. Plates
688 were incubated at 37 ˚C for 24 hours and then imaged. (**B**) Δ6 endo carrying the
689 indicated EP under control of an arabinose-inducible promoter was grown without IPTG
690 (chromosomal ShyA off) and with arabinose (pBAD33-encoded EP on) for 3 hours and
691 then imaged. Scale bar, 5 µm.

692

693 ## References

694 1. Espaillat A, Forsmo O, El Biari K, Bjork R, Lemaitre B, Trygg J, Canada FJ, de
695 Pedro MA, Cava F. 2016. Chemometric Analysis of Bacterial Peptidoglycan
696 Reveals Atypical Modifications That Empower the Cell Wall against Predatory
697 Enzymes and Fly Innate Immunity. J Am Chem Soc 138:9193-204.
698 2. Vollmer W, Bertsche U. 2008. Murein (peptidoglycan) structure, architecture and
699 biosynthesis in Escherichia coli. Biochim Biophys Acta 1778:1714-34.
700 3. Vollmer W, Blanot D, de Pedro MA. 2008. Peptidoglycan structure and
701 architecture. FEMS Microbiol Rev 32:149-67.
702 4. Dik DA, Fisher JF, Mobashery S. 2018. Cell-Wall Recycling of the Gram-
703 Negative Bacteria and the Nexus to Antibiotic Resistance. Chem Rev 118:5952-
704 5984.
705 5. Park JT, Uehara T. 2008. How bacteria consume their own exoskeletons
706 (turnover and recycling of cell wall peptidoglycan). Microbiol Mol Biol Rev 72:211-
707 27, table of contents.
708 6. Uehara T, Park JT. 2008. Growth of Escherichia coli: significance of
709 peptidoglycan degradation during elongation and septation. J Bacteriol 190:3914-
710 22.
711 7. Meeske AJ, Riley EP, Robins WP, Uehara T, Mekalanos JJ, Kahne D, Walker S,
712 Kruse AC, Bernhardt TG, Rudner DZ. 2016. SEDS proteins are a widespread
713 family of bacterial cell wall polymerases. Nature 537:634-638.
714 8. Paradis-Bleau C, Markovski M, Uehara T, Lupoli TJ, Walker S, Kahne DE,
715 Bernhardt TG. 2010. Lipoprotein cofactors located in the outer membrane
716 activate bacterial cell wall polymerases. Cell 143:1110-20.
717 9. Typas A, Banzhaf M, van den Berg van Saparoea B, Verheul J, Biboy J, Nichols
718 RJ, Zietek M, Beilharz K, Kannenberg K, von Rechenberg M, Breukink E, den
719 Blaauwen T, Gross CA, Vollmer W. 2010. Regulation of peptidoglycan synthesis
720 by outer-membrane proteins. Cell 143:1097-109.
721 10. Emami K, Guyet A, Kawai Y, Devi J, Wu LJ, Allenby N, Daniel RA, Errington J.
722 2017. RodA as the missing glycosyltransferase in Bacillus subtilis and antibiotic
723 discovery for the peptidoglycan polymerase pathway. Nat Microbiol 2:16253.
724 11. Dorr T, Lam H, Alvarez L, Cava F, Davis BM, Waldor MK. 2014. A novel
725 peptidoglycan binding protein crucial for PBP1A-mediated cell wall biogenesis in
726 Vibrio cholerae. PLoS Genet 10:e1004433.
727 12. Dorr T, Moll A, Chao MC, Cava F, Lam H, Davis BM, Waldor MK. 2014.
728 Differential requirement for PBP1a and PBP1b in in vivo and in vitro fitness of
729 Vibrio cholerae. Infect Immun 82:2115-24.
730 13. Dion MF, Kapoor M, Sun Y, Wilson S, Ryan J, Vigouroux A, van Teeffelen S,
731 Oldenbourg R, Garner EC. 2019. Bacillus subtilis cell diameter is determined by
732 the opposing actions of two distinct cell wall synthetic systems. Nat Microbiol
733 4:1294-1305.
734 14. Vigouroux A, Cordier B, Aristov A, Alvarez L, Ozbaykal G, Chaze T, Oldewurtel
735 ER, Matondo M, Cava F, Bikard D, van Teeffelen S. 2020. Class-A penicillin

binding proteins do not contribute to cell shape but repair cell-wall defects. Elife 9.

15. Vermassen A, Leroy S, Talon R, Provot C, Popowska M, Desvaux M. 2019. Cell Wall Hydrolases in Bacteria: Insight on the Diversity of Cell Wall Amidases, Glycosidases and Peptidases Toward Peptidoglycan. Front Microbiol 10:331.
16. Lee TK, Huang KC. 2013. The role of hydrolases in bacterial cell-wall growth. Curr Opin Microbiol 16:760-6.
17. Do T, Page JE, Walker S. 2020. Uncovering the activities, biological roles, and regulation of bacterial cell wall hydrolases and tailoring enzymes. J Biol Chem 295:3347-3361.
18. Vollmer W. 2012. Bacterial growth does require peptidoglycan hydrolases. Mol Microbiol 86:1031-5.
19. Hashimoto M, Ooiwa S, Sekiguchi J. 2012. Synthetic lethality of the lytE cwlO genotype in Bacillus subtilis is caused by lack of D,L-endopeptidase activity at the lateral cell wall. J Bacteriol 194:796-803.
20. Dorr T, Cava F, Lam H, Davis BM, Waldor MK. 2013. Substrate specificity of an elongation-specific peptidoglycan endopeptidase and its implications for cell wall architecture and growth of Vibrio cholerae. Mol Microbiol 89:949-62.
21. Singh SK, SaiSree L, Amrutha RN, Reddy M. 2012. Three redundant murein endopeptidases catalyse an essential cleavage step in peptidoglycan synthesis of Escherichia coli K12. Mol Microbiol 86:1036-51.
22. Meisner J, Montero Llopis P, Sham LT, Garner E, Bernhardt TG, Rudner DZ. 2013. FtsEX is required for CwlO peptidoglycan hydrolase activity during cell wall elongation in Bacillus subtilis. Mol Microbiol 89:1069-83.
23. Brunet YR, Wang X, Rudner DZ. 2019. SweC and SweD are essential co-factors of the FtsEX-CwlO cell wall hydrolase complex in Bacillus subtilis. PLoS Genet 15:e1008296.
24. Carballido-Lopez R, Formstone A, Li Y, Ehrlich SD, Noirot P, Errington J. 2006. Actin homolog MreBH governs cell morphogenesis by localization of the cell wall hydrolase LytE. Dev Cell 11:399-409.
25. Dominguez-Cuevas P, Porcelli I, Daniel RA, Errington J. 2013. Differentiated roles for MreB-actin isologues and autolytic enzymes in Bacillus subtilis morphogenesis. Mol Microbiol 89:1084-98.
26. Tomasz A. 1979. The mechanism of the irreversible antimicrobial effects of penicillins: how the beta-lactam antibiotics kill and lyse bacteria. Annu Rev Microbiol 33:113-37.
27. Schneider T, Sahl HG. 2010. An oldie but a goodie - cell wall biosynthesis as antibiotic target pathway. Int J Med Microbiol 300:161-9.
28. Lai GC, Cho H, Bernhardt TG. 2017. The mecillinam resistome reveals a role for peptidoglycan endopeptidases in stimulating cell wall synthesis in Escherichia coli. PLoS Genet 13:e1006934.
29. Kitano K, Tuomanen E, Tomasz A. 1986. Transglycosylase and endopeptidase participate in the degradation of murein during autolysis of Escherichia coli. J Bacteriol 167:759-65.
30. Dorr T, Davis BM, Waldor MK. 2015. Endopeptidase-mediated beta lactam tolerance. PLoS Pathog 11:e1004850.

31. Singh SK, Parveen S, SaiSree L, Reddy M. 2015. Regulated proteolysis of a cross-link-specific peptidoglycan hydrolase contributes to bacterial morphogenesis. Proc Natl Acad Sci U S A 112:10956-61.
32. Banzhaf M, Yau HC, Verheul J, Lodge A, Kritikos G, Mateus A, Cordier B, Hov AK, Stein F, Wartel M, Pazos M, Solovyova AS, Breukink E, van Teeffelen S, Savitski MM, den Blaauwen T, Typas A, Vollmer W. 2020. Outer membrane lipoprotein NlpI scaffolds peptidoglycan hydrolases within multi-enzyme complexes in Escherichia coli. EMBO J 39:e102246.
33. Srivastava D, Seo J, Rimal B, Kim SJ, Zhen S, Darwin AJ. 2018. A Proteolytic Complex Targets Multiple Cell Wall Hydrolases in Pseudomonas aeruginosa. mBio 9.
34. Shin JH, Sulpizio AG, Kelley A, Alvarez L, Murphy SG, Fan L, Cava F, Mao Y, Saper MA, Dorr T. 2020. Structural basis of peptidoglycan endopeptidase regulation. Proc Natl Acad Sci U S A 117.
35. Koch AL. 1998. The three-for-one model for gram-negative wall growth: a problem and a possible solution. FEMS Microbiol Lett 162:127-34.
36. Höltje JV. 1993. "Three for one" - a Simple Growth Mechanism that Guarantees a Precise Copy of the Thin, Rod-Shaped Murein Sacculus of *Escherichia coli*. *In* de Pedro MA, Höltje JV, Löffelhardt W (ed), Bacterial Growth and Lysis. Springer, Boston, MA.
37. Chodisetti PK, Reddy M. 2019. Peptidoglycan hydrolase of an unusual cross-link cleavage specificity contributes to bacterial cell wall synthesis. Proc Natl Acad Sci U S A 116:7825-7830.
38. Denome SA, Elf PK, Henderson TA, Nelson DE, Young KD. 1999. Escherichia coli mutants lacking all possible combinations of eight penicillin binding proteins: viability, characteristics, and implications for peptidoglycan synthesis. J Bacteriol 181:3981-93.
39. Kuru E, Hughes HV, Brown PJ, Hall E, Tekkam S, Cava F, de Pedro MA, Brun YV, VanNieuwenhze MS. 2012. In Situ probing of newly synthesized peptidoglycan in live bacteria with fluorescent D-amino acids. Angew Chem Int Ed Engl 51:12519-23.
40. Cava F, de Pedro MA, Lam H, Davis BM, Waldor MK. 2011. Distinct pathways for modification of the bacterial cell wall by non-canonical D-amino acids. EMBO J 30:3442-53.
41. Culp EJ, Waglechner N, Wang W, Fiebig-Comyn AA, Hsu YP, Koteva K, Sychantha D, Coombes BK, Van Nieuwenhze MS, Brun YV, Wright GD. 2020. Evolution-guided discovery of antibiotics that inhibit peptidoglycan remodelling. Nature 578:582-587.
42. Blackman SA, Smith TJ, Foster SJ. 1998. The role of autolysins during vegetative growth of Bacillus subtilis 168. Microbiology 144 (Pt 1):73-82.
43. Takacs CN, Poggio S, Charbon G, Pucheault M, Vollmer W, Jacobs-Wagner C. 2010. MreB drives de novo rod morphogenesis in Caulobacter crescentus via remodeling of the cell wall. J Bacteriol 192:1671-84.
44. Ostash B, Walker S. 2010. Moenomycin family antibiotics: chemical synthesis, biosynthesis, and biological activity. Nat Prod Rep 27:1594-617.

45. Cross T, Ransegnola B, Shin JH, Weaver A, Fauntleroy K, VanNieuwenhze MS, Westblade LF, Dorr T. 2019. Spheroplast-Mediated Carbapenem Tolerance in Gram-Negative Pathogens. Antimicrob Agents Chemother 63.
46. Dominguez-Escobar J, Chastanet A, Crevenna AH, Fromion V, Wedlich-Soldner R, Carballido-Lopez R. 2011. Processive movement of MreB-associated cell wall biosynthetic complexes in bacteria. Science 333:225-8.
47. van Teeffelen S, Wang S, Furchtgott L, Huang KC, Wingreen NS, Shaevitz JW, Gitai Z. 2011. The bacterial actin MreB rotates, and rotation depends on cell-wall assembly. Proc Natl Acad Sci U S A 108:15822-7.
48. Garner EC, Bernard R, Wang W, Zhuang X, Rudner DZ, Mitchison T. 2011. Coupled, circumferential motions of the cell wall synthesis machinery and MreB filaments in B. subtilis. Science 333:222-5.
49. Billaudeau C, Chastanet A, Yao Z, Cornilleau C, Mirouze N, Fromion V, Carballido-Lopez R. 2017. Contrasting mechanisms of growth in two model rod-shaped bacteria. Nat Commun 8:15370.
50. Heidrich C, Templin MF, Ursinus A, Merdanovic M, Berger J, Schwarz H, de Pedro MA, Holtje JV. 2001. Involvement of N-acetylmuramyl-L-alanine amidases in cell separation and antibiotic-induced autolysis of Escherichia coli. Mol Microbiol 41:167-78.
51. Moll A, Dorr T, Alvarez L, Chao MC, Davis BM, Cava F, Waldor MK. 2014. Cell separation in Vibrio cholerae is mediated by a single amidase whose action is modulated by two nonredundant activators. J Bacteriol 196:3937-48.
52. Wientjes FB, Nanninga N. 1991. On the role of the high molecular weight penicillin-binding proteins in the cell cycle of Escherichia coli. Res Microbiol 142:333-44.
53. Cho H, Wivagg CN, Kapoor M, Barry Z, Rohs PDA, Suh H, Marto JA, Garner EC, Bernhardt TG. 2016. Bacterial cell wall biogenesis is mediated by SEDS and PBP polymerase families functioning semi-autonomously. Nat Microbiol 1:16172.
54. Dik DA, Marous DR, Fisher JF, Mobashery S. 2017. Lytic transglycosylases: concinnity in concision of the bacterial cell wall. Crit Rev Biochem Mol Biol 52:503-542.
55. Cai L, Friedman N, Xie XS. 2006. Stochastic protein expression in individual cells at the single molecule level. Nature 440:358-62.
56. Heidelberg JF, Eisen JA, Nelson WC, Clayton RA, Gwinn ML, Dodson RJ, Haft DH, Hickey EK, Peterson JD, Umayam L, Gill SR, Nelson KE, Read TD, Tettelin H, Richardson D, Ermolaeva MD, Vamathevan J, Bass S, Qin H, Dragoi I, Sellers P, McDonald L, Utterback T, Fleishmann RD, Nierman WC, White O, Salzberg SL, Smith HO, Colwell RR, Mekalanos JJ, Venter JC, Fraser CM. 2000. DNA sequence of both chromosomes of the cholera pathogen Vibrio cholerae. Nature 406:477-83.
57. Mekalanos JJ. 1983. Duplication and amplification of toxin genes in Vibrio cholerae. Cell 35:253-63.
58. Dalia AB. 2018. Natural Cotransformation and Multiplex Genome Editing by Natural Transformation (MuGENT) of Vibrio cholerae. Methods Mol Biol 1839:53-64.

59. Guzman LM, Belin D, Carson MJ, Beckwith J. 1995. Tight regulation, modulation, and high-level expression by vectors containing the arabinose PBAD promoter. J Bacteriol 177:4121-30.
60. Chin CS, Sorenson J, Harris JB, Robins WP, Charles RC, Jean-Charles RR, Bullard J, Webster DR, Kasarskis A, Peluso P, Paxinos EE, Yamaichi Y, Calderwood SB, Mekalanos JJ, Schadt EE, Waldor MK. 2011. The origin of the Haitian cholera outbreak strain. N Engl J Med 364:33-42.
61. Gibson DG, Young L, Chuang RY, Venter JC, Hutchison CA, 3rd, Smith HO. 2009. Enzymatic assembly of DNA molecules up to several hundred kilobases. Nat Methods 6:343-5.
62. Donnenberg MS, Kaper JB. 1991. Construction of an eae deletion mutant of enteropathogenic Escherichia coli by using a positive-selection suicide vector. Infect Immun 59:4310-7.
63. Tinevez JY, Perry N, Schindelin J, Hoopes GM, Reynolds GD, Laplantine E, Bednarek SY, Shorte SL, Eliceiri KW. 2017. TrackMate: An open and extensible platform for single-particle tracking. Methods 115:80-90.
64. Tarantino N, Tinevez JY, Crowell EF, Boisson B, Henriques R, Mhlanga M, Agou F, Israel A, Laplantine E. 2014. TNF and IL-1 exhibit distinct ubiquitin requirements for inducing NEMO-IKK supramolecular structures. J Cell Biol 204:231-45.
65. Bacher CP, Reichenzeller M, Athale C, Herrmann H, Eils R. 2004. 4-D single particle tracking of synthetic and proteinaceous microspheres reveals preferential movement of nuclear particles along chromatin - poor tracks. BMC Cell Biol 5:45.
66. Alvarez L, Hernandez SB, de Pedro MA, Cava F. 2016. Ultra-Sensitive, High-Resolution Liquid Chromatography Methods for the High-Throughput Quantitative Analysis of Bacterial Cell Wall Chemistry and Structure. Methods Mol Biol 1440:11-27.
67. Madeira F, Park YM, Lee J, Buso N, Gur T, Madhusoodanan N, Basutkar P, Tivey ARN, Potter SC, Finn RD, Lopez R. 2019. The EMBL-EBI search and sequence analysis tools APIs in 2019. Nucleic Acids Res 47:W636-W641.